Dye-Sensitized Solar Cells Based on Electrospun Ag-doped TiO_2/PVA Nanofibers

Van-Pham, Dan Thuy; Noc Mai, Ngo Truong; Thi Bich Quyen, Thi; Hong Ngoc, Nguyen; Bao Long, Tran Vu; Than Ngan, Thi Thao; Hong Thien, Doan Van*[+]

Department of Chemical Engineering, Can Tho University–3/2 Street, Ninh Kieu District, Can Tho City, VIETNAM

Don Ngoc, Ta

School of Chemical Engineering, Hanoi University of Science and Technology, Dai Co Viet, Hanoi, 10000, Vietnam; Ministry of Education and Training, Ha Noi City, 570000, VIETNAM

Minh Nhan, Le

Department of Chemistry, Faculty of Basic Sciences, Can Tho University of Medicine and Pharmacy, 179 Nguyen Van Cu Street, Ninh Kieu District, Can Tho City, VIETNAM

ABSTRACT: *Ag-doped TiO_2/PVA nanofibers have many potential applications as a photoanode of dye-sensitized solar cells (DSSCs). In this study, we report the fabrication of DSSCs based on Ag-doped TiO_2/PVA nanofibers as photoanode, graphene oxide as a Pt-free counter electrode catalyst, and natural dye sensitizer. Ag-doped TiO_2/PVA nanofibers were fabricated using an electrospinning method. The electrospun nanofibers were characterized by a scanning electron microscope, X-ray diffraction, Fourier transform infrared spectroscopy and thermogravimetric analysis. The nanoparticle content of lower 100 mg/mL, and the electrospun nanofibers were uniform. Based on the results of the characterization analysis, the electrospun Ag-doped TiO_2/PVA nanofibers were successfully prepared with diameters from 100 to 400 nm. They were used as photoanodes of DSSCs using a natural dye sensitizer extracted from the leaf of the magenta plant. The highest power conversion efficiency of DSSCs with Ag-doped TiO_2/PVA nanofibers was 0.6% from the J-V curves. This approach would be a potential application for fabricating a solar cell based on composite fiber, Pt-free catalyst, and natural dye sensitizer.*

KEYWORDS: *Ag-doped TiO_2 nanoparticles; Ag-doped TiO_2/PVA nanofibers; Dye-sensitized solar cells; Electrospinning.*

INTRODUCTION

The solar cell is produced to replace fossil fuels with renewable energy sources. The energy demand is increasing worldwide due to the rapid growth of the population. Therefore, electricity generation uses renewable energy sources such as solar energy [1-6]. Electricity generation uses renewable energy sources such as solar

***** *To whom correspondence should be addressed.*
+ *E-mail: dvhthien@ctu.edu.vn*
1021-9986/2023/5/1399-1409 11/$/6.01

energy from the sun, geothermal energy from the heat inside the earth, wind energy, biomass from plants, and hydropower from flowing water. Among the renewable energy sources, electricity from solar power is a significant energy source in clean energy production. Dye-sensitized solar cells (DSSCs) technology consists of a nanostructured semiconductor anode, a photosensitizer, a redox electrolyte, and a cathode. The efficiency of these devices not only depends on the properties of the dye and redox types of electrolytes but also on the interaction between the photocathodes and photoanodes. Each factor greatly impacts the DSSCs efficiency [1, 2, 4-11].

Of the known semiconductors, TiO_2 is a promising candidate as a photoanode material for DSSCs due to its chemical stability, high redox ability, low cost, and non-toxicity [3, 12-19]. To improve the efficiency of solar cells, TiO_2 photoanode films have been explored with various morphologies and dopants [20-23]. Some metal NanoParticles (NPs) such as Au, Ag, or Pt have attracted more attention due to their Surface Plasmon Effect (SPR) [19, 24-31]. Ag is one of the promising materials among metal NPs due to its SPR property in the visible region. The surface plasmonic resonance feature provides several benefits. First, it aids the dyes in absorbing the light better. Ag NPs operate as electron sinks, decreasing charge recombination and enhancing the electron transfer process. Furthermore, the surface area of the Ag-doped TiO_2 sheet influences the photovoltaic performance of DSSCs [8-10]. When the film has a higher surface area, more dye molecules can be attached efficiently, resulting in improved velocity of generating electrons. The utilization of a 1D nanostructure in the shape of the fiber is one viable way to increase the surface area of Ag-doped TiO_2 films.

The cathode works like a receptor for the electrons sent by the photoanode. The platinum cathode is generally used due to its excellent conductivity and electrocatalytic activity. However, platinum is too expensive to be produced on a large industrial scale [8-10]. Graphene Oxide (GO) is a great choice for its low cost. Thus, this study aimed to prepare DSSCs based on Ag-doped TiO_2/PVA nanofibers as a photoelectrode, GO as a Pt-free counter electrode catalyst, and natural dye sensitizer.

Anthocyanin is the main component of several plants, flowers, and fruits and gives efficient performances in photosensitization [3, 18, 32-35]. In this study, the natural dye extracted from the leaf of the magenta plant was used for DSSCs. Polyvinyl alcohol (PVA) was selected for electrospinning with different amounts of Ag-doped TiO_2 NPs. The electrospun Ag-doped TiO_2 nanofibers were used as a photoanode. Synthesized GO by the Hummers method reported in the previous paper was used as a catalyst [36]. Then, the photovoltaic performance of DSSCs was presented by the J-V plot.

EXPERIMENTAL SECTION

Materials

Nitric acid (HNO_3, 65%), sulfuric acid (H_2SO_4, 98%), potassium iodide (KI, 99%), iodine (I_2), titanium dioxide (TiO_2, 99.9%), silver nitrate ($AgNO_3$, 99.8%), ethanol (C_2H_5OH, 100%), polyvinyl alcohol (PVA, Mw 146,000-186,000, 99% hydrolyzed), potassium permanganate ($KMnO_4$, 99.5%), hydrogen peroxide (H_2O_2, 30%), titanium butoxide ($Ti(OBu)_4$, 97%), and cis-bis (isothiocyanato) bis (2,2′-bipyridyl-4,4′-dicarboxylato) ruthenium (II)-N719 were purchased from Sigma. Sodium hydroxide (NaOH, 100%) and hydrochloric acid (HCl, 36.5%) were purchased from Merck. Ammonium hydroxide (NH_4OH, 25%) was obtained from Xilong. Fluorine-doped tin oxide (FTO) coated glass substrates were purchased from Pilkington with a sheet resistance of ohms per square (15 Ω/sq). Distilled water was used for all the experiments.

Methods

Synthesis Ag-doped TiO_2 NPs

As reported in previous work, the Ag-doped TiO_2 NPs were prepared using the sol-gel method. 5.0 g of $Ti(OBu)_4$ was added dropwise under magnetic stirring to 300 mL of HCl solution (0.5 M). Then, NH_4OH (1 M) was slowly added to the above solution. The pH of the solution was kept at 8.0. After aging for 30 min, the gel was washed with DI water several times and filtered to remove chloride ions.

The as-prepared gel was dispersed in 100 mL of H_2O under stirring for 30 min at room temperature. H_2O_2 was added to the suspension until the solution color changed to light orange. $AgNO_3$ solution was added into the suspension with the molar ratios of $AgNO_3$:H_2O_2:TiO_2 were 0.0037:2:1 under stirring for 3 hours. The mixture was then heated at 90 °C for 8 hours. The pH of the mixture was adjusted to 7 with NH_4OH solution (1 M). The suspension was washed several times with DI water to remove the impurity components by centrifugation.

Preparation of electrospun Ag-doped TiO_2/PVA nanofibers

PVA was dissolved in 1 mL of deionized water at 80 °C for 5 hours to obtain the PVA solution (11 wt%). Next, the amount of Ag-doped TiO_2 NPs with different contents of 60 mg, 80 mg, 100 mg, and 120 mg was added under stirring for 1 hour. After stabilizing for 24 hours, the electrospinning experiments were conducted to determine the optimal conditions of Ag-doped TiO_2 NPs amount.

The electrospinning was performed on a homemade setup. The electrospinning experiments were carried out at suitable conditions, including 0.6 mL/h of flow rate, 15 cm of tip-to-collector distance, and 15 kV of applied voltage.

Characterizations of Ag-doped TiO_2 NPs and Ag-doped TiO_2/PVA nanofibers

The band-gap energy of Ag-doped TiO_2 NPs was determined using the Tauc plot equation. The Tauc plot equation was plotted based on the UV-Vis spectra (The UV-1800 Shimadzu spectrophotometer, Japan). The formation and crystalline phase of Ag-doped TiO_2 NPs were detected by X-ray diffraction (XRD, D8 Phaser, Advance Brucker, Germany) using CuKα radiation (λ = 1.5406 Å). Data were obtained over 2 theta (2θ) ranging from 10 to 80° with a scanning rate of 0.05°/min. The surface morphology of the NPs and nanofibers was observed by a scanning electron microscope (SEM, FE-SEM S4800 Hitachi, Japan) at an accelerating voltage of 10 kV after gold coating. The size of Ag-doped TiO_2 NPs was determined by a Transmission Electron Microscope (TEM, JEOL JEM-1400, Japan) with an accelerating voltage of 100 kV. The chemical interactions between PVA and HA were observed by Fourier Transform InfraRed spectroscopy (FT-IR, FT-NIR/MIR spectrometer Frontier, USA) using KBr pellets. The spectra were scanned over 4000 – 400 cm^{-1}. Thermal-Gravimetric Analysis (TGA, LabSys Evo TG-DSC 1600, France) was used to determine the weight loss of Ag-doped TiO_2/PVA nanofibers. Approximately 5 mg of the nanofibers was loaded into an aluminum oxide crucible and heated from room temperature to 1000 °C. The heating rate was 10 °C/min with a nitrogen gas flow rate of 10 mL/min.

Assembly and evaluation of DSSCs

Preparation of natural dye: Magenta leaves (5 g) were dried to saturated moisture content and stirred in 30 mL of ethanol/H_2O (1:1) solvent at 80 ºC for 30 min. The absorption properties of the anthocyanins extracted from magenta leaves were measured by a UV-Visible spectrometer (Thermo Scientific Evolution 60S, USA) with a spectral range of 350 nm – 800 nm.

Preparation of electrolyte solution: Synthesizing the I^-/I^-_3 electrolyte solution was performed in low light conditions. Namely, 0.127 g of I_2 was slowly added to 10 mL of ethylene glycol. The solution was stirred for 30 min. Then, 0.83 g of KI was added to the above solution and stirred for 30 minutes to obtain the electrolyte solution.

For electrodes: FTO glasses (1 cm × 1 cm) were washed with ethanol, then immersed in HCl (0.1 M) in the ultrasonic tank for 15 min. Then, FTO glasses were washed with distilled water and dried. Ag-doped TiO_2/PVA nanofibers were prepared by an electrospinning method. The time for the electrospun Ag-doped TiO_2/PVA nanofibers to be deposited on the electrode was 10 min. The nanofibers were directly covered on the conductivity side of clean FTO glasses, followed by sintering at 450 ºC for 45 min. After the dye adsorption (natural dye or 0.5 mM N719 dye) at room temperature for 15 hours, the working electrode and the counter electrode (FTO glass with GO catalyst) were sealed with a double clip. Finally, the electrolyte solution was injected into the cell. The cell performance was evaluated with a solar simulator (SAN-EI electric Japan, XES-40S3) used to simulate sunlight with a capacity of 100 mW/cm^2. The J-V curves were obtained from the photoelectric measurement of the device (Tektronix US, Keithley 2450) with an active area of 0.36 cm^2.

RESULTS AND DISCUSSION

Characterization of Ag-doped TiO_2 NPs

The band-gap energy

Fig. 1 shows the band-gap energy determined from the UV-Vis spectra of Ag-doped TiO_2 NPs with various Ag concentrations. The absorption wavelength of TiO_2 NPs at 381 nm (corresponding to 3.25 eV) moved to a longer wavelength (corresponding with the decrease of band-gap energy) after doping with Ag concentrations of 0.25%, 0.5%, 0.75%, and 1%, showing the band-gap energies of 3.06 eV, 2.9 eV, 2.67 eV, and 2.33 eV, respectively. With a concentration of 0.25% Ag (corresponding to 3.06 eV), the visible light at 405 nm wavelength was absorbed. Moreover, the more silver doped inside the structure of TiO_2, the easier the material is oxidized. Therefore, a concentration of 0.25% Ag was chosen as the optimal condition.

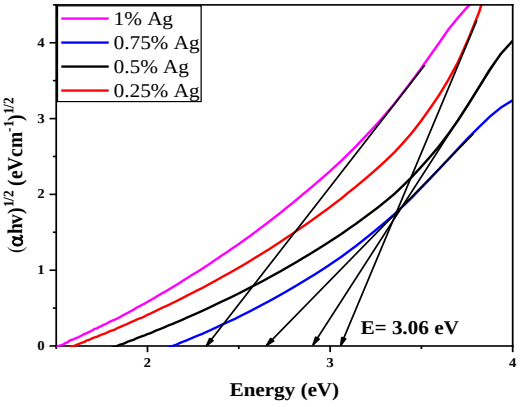

Fig. 1: Band-gap energy is obtained by extrapolating the linear portion of the (αhν)1/2 versus photon energy (eV) curve.

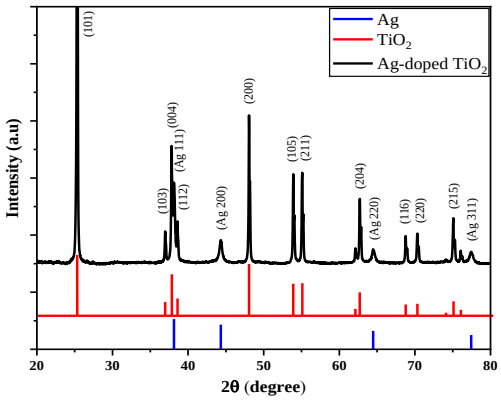

Fig. 2: The X-ray diffraction pattern of synthesized Ag-doped TiO_2 NPs.

The XRD results

Fig. 2 shows the X-ray diffraction patterns of Ag-doped TiO_2 materials. The characteristic diffraction peaks at 2 theta 25.3°, 36.9°, 37.8°, 38.5°, 48.1°, 54.0°, 55.1°, 62.1°, and 75.0° corresponding to the lattice planes (101), (103), (004), (112), (200), (105), (211), (204), and (215), respectively for the anatase phase, which coincided with JCPDS card no. 21-1272. The new peaks of (111), (200), (220), and (311) confirmed the presence of Ag NPs in comparison with the standard data (JCPDS card no: 89-3722). In addition, the diffraction peaks corresponding to the rutile phase of TiO_2 also appeared on the pattern. From the calculation of the result of XRD diffraction, the crystallinity percentage is relatively high (79.2%). Amorphous or semicrystalline TiO_2 is usually unstable in the structure. It leads to easy destruction of the TiO_2 structure when DSSC exposure to the high temperature of sunlight. Therefore, the high crystalline structure TiO_2 is always required to improve the DSSC performance. In addition, the phase composition of TiO_2 can be determined using Equation (1) [37]:

$$W_A = \frac{1}{1+1.265\left(\frac{I_R}{I_A}\right)} \quad (1)$$

Where W_A, I_A, and I_R denote the anatase weight percentage, and the intensity of the strongest anatase and rutile reflection, respectively.

The calculated results of W_A for pure TiO_2 and synthesized Ag-doped TiO_2, indicate that Ag-doped TiO_2 has W_A values of 92.1%, higher than that of pure TiO_2 (69.90%) [37], which increases the DSSC performance. The anatase has higher photocatalytic activity because of contains more defects and vacancies, which can produce more oxygen vacancies to capture electrons. Rutile is the most stable crystalline structure with fewer defects, and this leads to the easy recombination of electrons and holes. Hence it has poor photocatalytic activity as compared to anatase.

FE-SEM, TEM results of Ag-doped TiO_2 NPs

The FE-SEM, TEM images, and the size distribution of Ag-doped TiO_2 NPs are shown in Fig. 3. The SEM images of the Ag-doped TiO_2 NPs illustrated poor dispersion and apparent aggregation. However, the rough surface morphology helps improve the photovoltaic performance by increasing the surface area. The TEM image shows that the Ag-doped TiO_2 NPs are spherical. The average particle size is 7.85 ± 1.06 nm in the size distribution.

Characterization of Ag-doped TiO_2/ PVA nanofibers

SEM results

Fig. 4 shows the different morphology of PVA fibers for the various concentrations of Ag-doped TiO_2 NPs in the solution. The Ag-doped TiO_2/PVA nanofibers were successfully synthesized under the optimal experimental conditions including PVA concentration of 11 wt%, a tip-to-collector distance of 15 cm, and an applied voltage of 15 kV. When an increase in the amount of the Ag-doped TiO_2 NPs from 60 to 100 mg/mL, electrospun Ag-doped TiO_2/PVA nanofibers are homogeneous (Fig. 4a-c). With the Ag-doped TiO_2 NPs content of 120 mg/mL, large beads appeared in the nanofibers (Fig. 4d). Therefore,

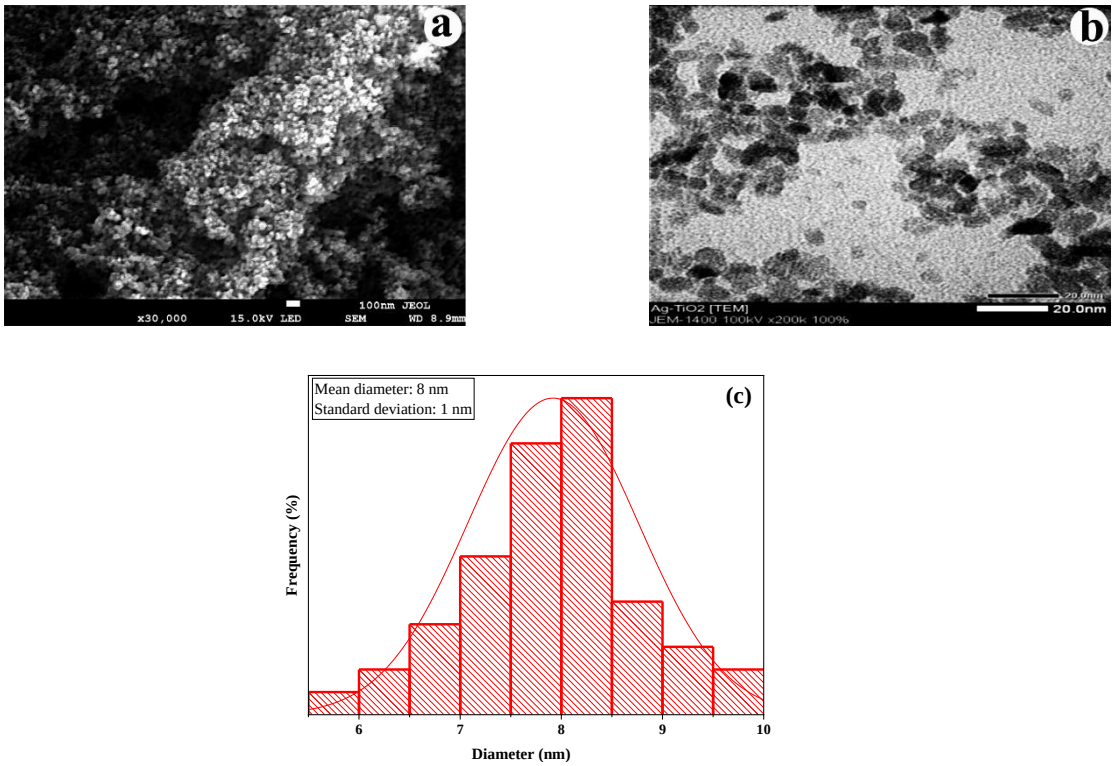

Fig. 3: (a) The FE-SEM, (b) TEM images, and (c) the size distribution of Ag-doped TiO_2 NPs.

we chose the content of Ag-doped TiO_2 NPs to be 60, 80, and 100 mg/mL for DSSCs applications. The results show that when the amount of Ag-doped TiO_2 NP increases, the power conversion efficiency of DSSCs increases. Thus, 100 mg/mL of Ag-doped TiO_2 NPs was chosen as the optimal condition.

The XRD results

Fig. 5 shows the X-Ray diffraction patterns of synthesized Ag-doped TiO_2/PVA nanofibers. The typical peaks of anatase TiO_2 were referenced from the Joint Committee on Powder Diffraction Standard (JCPDS No. 21-1272). Furthermore, some of the typical peaks as (111) and (200) confirmed the presence of Ag NPs. While the new peak at $2\theta = 19.44°$ indicates the presence of PVA. The X-ray diffraction pattern indicates that the Ag-doped TiO_2/PVA nanofibers have been successfully prepared. In addition, the interactions between the hydroxyl groups of PVA and Ag-doped TiO_2 NPs lead to a decrease in intermolecular interaction between PVA chains. Therefore, the intensity of Ag-doped TiO_2/PVA nanofibers decreases compared to Ag-doped TiO_2 NPs.

The FT-IR results

Fig. 6 shows the FT-IR spectra of Ag-doped TiO_2 NPs, PVA, and synthesized Ag-doped TiO_2/PVA nanofibers with a wavelength range of 4000–400 cm^{-1}. In Fig. 6b, the peaks in the range of 800–400 cm^{-1} represent O–Ti–O bonding. Remarkedly, the signals at 732, 652, and 479 cm^{-1} are assigned to be anatase [38]. The peaks at 1627 cm^{-1} and 3416 cm^{-1} are the characteristics of δ-H_2O bending and vibration of hydroxyl groups, respectively [39]. Meanwhile, the peak at 1384 cm^{-1} (peak 3) indicates the Ag-O-Ti bonding [40].

In Fig. 6c, the high intense bands positioned around 3477 cm^{-1} correspond to O–H stretching vibrations of the hydroxyl group. The absorption bands at 2911 cm^{-1} are assigned to the carbon-hydrogen (-CH_2-) bond stretching. The absorption peaks are observed at 1727 cm^{-1}, due to C–O bonds, which is a typical peak for PVA. The peaks at 1141 and 856 cm^{-1} indicated C-O-H and C-C stretching vibrations of PVA, respectively. The absorption bands positioned around 400–800 cm^{-1} are for O–Ti–O bonding. The typical peak at 1384 cm^{-1} proposes the official of Ag-O-Ti individually.

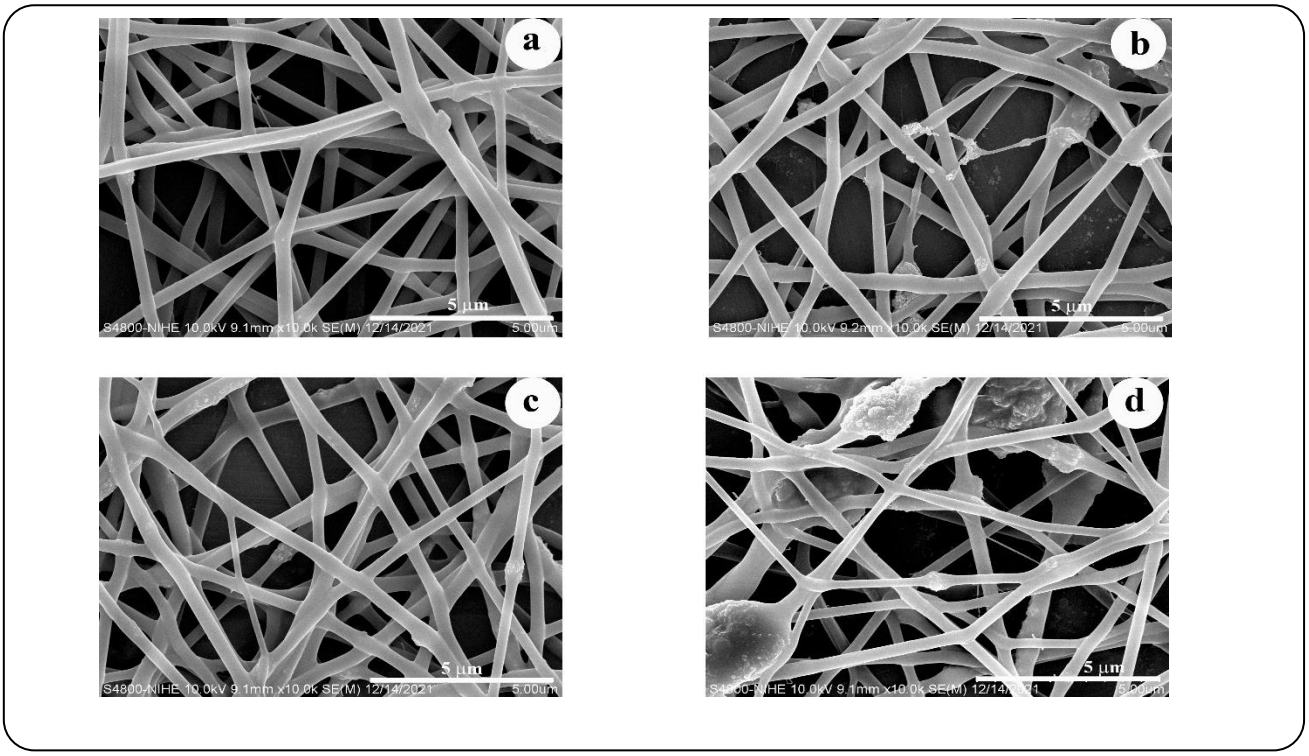

Fig. 4: SEM images of Ag-doped TiO2/PVA nanofibers with different concentrations of Ag-doped TiO2 NPs: (a) 60 mg/mL, (b) 80 mg/mL, (c) 100 mg/mL, and (d) 120 mg/mL.

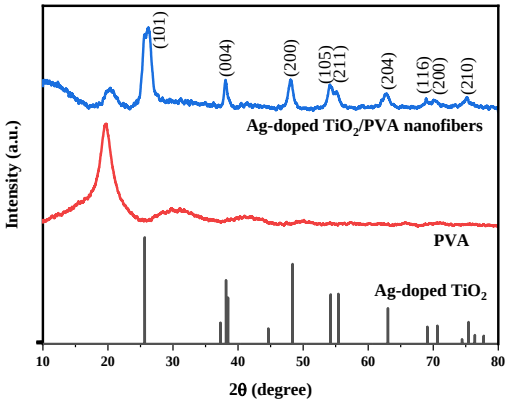

Fig. 5: The X-ray diffraction patterns of synthesized PVA/Ag-doped TiO2 nanofibers.

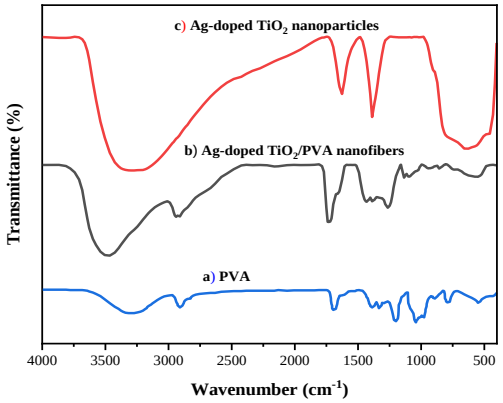

Fig. 6: FT-IR spectra of (a) PVA, (b) Ag-doped TiO2/PVA NPs, and (c) Ag-doped TiO2/PVA nanofibers.

The TGA results

The DTG-TGA curves of as-prepared Ag-doped TiO_2/PVA nanofibers are shown in Fig. 7. In the TGA curves, the mass loss occurs in four stages with the temperature ranging from 50 to 1000 °C. In Fig. 7, the endothermic peak at about 99.8 °C is due to the desorption of adsorbed water. The mass lost at stage (I) is about 6.76 wt% in the TGA curve. The decomposition of PVA occurs in the temperature range of 200–500 °C. The mass lost at stages (II) and (III) is approximately 32.01 wt% and 7.94 wt%, respectively due to the dehydration reaction of –OH groups and C-C linking in PVA chains. Finally, the mass loss of stage (IV) is 1.25 wt% in the temperature range of 600–800 °C, which may be ascribed to the decomposition of impurities. The mass remaining after pyrolysis is that of Ag-doped TiO_2 NPs due to the thermal stability of the material.

Table 1: Photovoltaic performance of DSSCs.

Materials	J_{SC} (mA/cm^2)	V_{OC} (V)	FF	η (%)
Ag-doped TiO_2/PVA nanofibers (60 mg/mL)	0.50	0.22	0.66	0.07
Ag-doped TiO_2/PVA nanofibers (80 mg/mL)	0.75	0.35	0.65	0.17
Ag-doped TiO_2/PVA nanofibers (100 mg/mL)	1.60	0.55	0.67	0.6
Ag-doped TiO_2/PVA nanofibers (100 mg/mL)- N719 dye	2.17	0.7	0.59	0.9

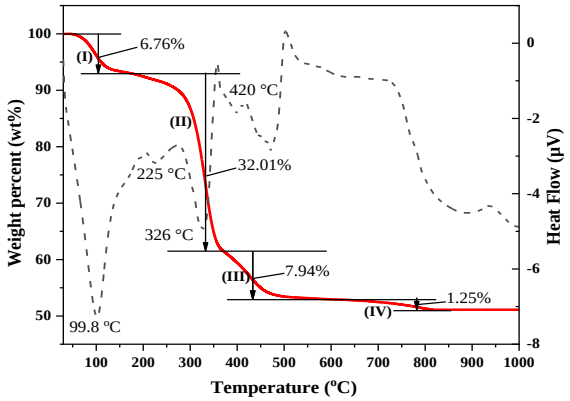

Fig. 5: The DTG–TGA curves of electrospun Ag-doped TiO2/PVA nanofibers.

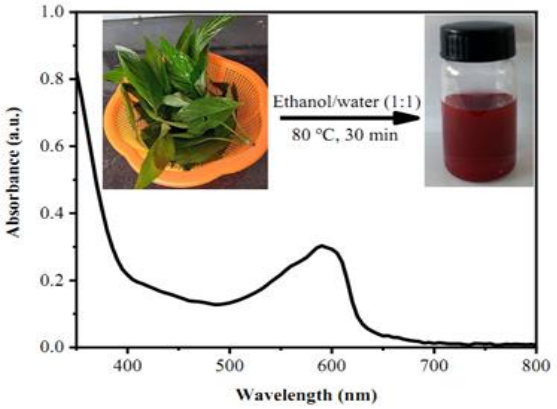

Fig. 6: UV-Vis absorption spectrum of natural pigment extracted from the magenta plant using the solvent of ethanol/water.

The photovoltaic study

Fig. 8 shows the UV-Vis spectrum of natural dye extracted from the magenta plant. The main component of the extract is anthocyanin [35]. Anthocyanin components absorb the wavelength in a range of 500 – 600 nm. The maximum absorption peak at 588 nm, is in good agreement with that of anthocyanin pigment. The band-gap energy (E_g) of natural dye was determined using Equation (2) [41].

$$E_g = \frac{hc}{\lambda_{max}} = \frac{1240\ (eV)}{\lambda_{max}} \quad (2)$$

Where *h* is the plank constant; *c* is the speed of light; λ_{max} is the wavelength of the maximum absorption peak of dye extract (588 nm). The calculated band-gap energy of extract dye was 2.1 eV, proper for light capturing at the visible region. Moreover, the anthocyanin molecules in dye extract have the -C=O and -OH groups, which can be bound to TiO_2. Thus, anthocyanin can promote electron transfer from the dye to the conduction band of the TiO_2 layer, increasing the power conversion efficiency of DSSCs.

Fig. 9 and Table 1 illustrate the J-V plot and the values for the DSSCs using the dye extracted from the magenta plant or N719 dye. In the case of Ag-doped TiO_2/ PVA nanofibers anode, when the amount of Ag-doped TiO_2 NPs increases in the fibers, the photovoltaic performance of DSSCs essentially increases. The short-circuit current density (J_{SC}) and open-circuit voltages (V_{OC}) are enhanced gradually with the increasing Ag-doped TiO_2 contents. Particularly, the Ag-doped TiO_2/PVA nanofibers (100 mg/mL) photoanode exhibited the highest J_{SC} and V_{OC} to 1.6 mA/cm^2 and 0.55 V, corresponding to the power conversion efficiency of 0.6%. The surface plasmon resonance property of Ag-doped TiO_2 NPs plays a crucial role in the improvement yield of DSSCs. First, the surface plasmon resonance property would decrease the band-gap energy of Ag-doped TiO_2. Second, the electric field of the surface plasmon resonance promotes the transport of photoelectrons from excited molecules to the TiO_2 semiconductor [42]. Finally, metal plasmon is located between TiO_2 semiconductor and anthocyanin molecules leading to the formation of the Schottky barrier, which could act as an electron sink, preventing the electron-hole

recombination. Moreover, the electrospinning method can generate hollow and mesoporous structures within each fiber, which increases the active surface area of Ag-doped TiO_2 NPs. The higher surface area allows better electrolytes resulting in faster electron diffusion and shortening the electron collection time [43]. With N719 dye, the power conversion efficiency is 0.9% higher than that with the dye extracted from the magenta plant. However, N719 industry standard dye has a high cost as well as causes environmental pollution.

Table 2: DSSCs based on different types of electrodes and catalysts.

Material	η (%)	Ref
TiO_2 coated – C (Anthocyanin)	0.56	[44]
TiO_2 coated – Pt (Anthocyanin)	0.55	[45]
PVA/Ag-doped TiO_2 fiber – GO (Anthocyanin)	0.6	This work

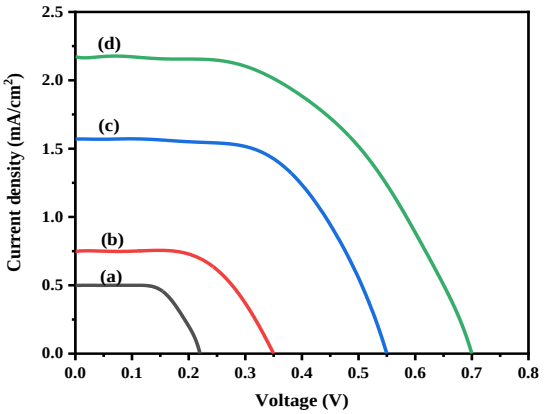

Fig. 9: The current density-voltage curves for DSSCs sensitized using the natural dye extracted from magenta plant with various amounts of Ag-doped TiO_2 NPs: (a) 60 mg/mL, (b) 80 mg/mL, (c) 100 mg/mL, and (d) 100 mg Ag-doped TiO_2 NPs /mL and N719 dye.

Table 2 shows the photovoltaic performance of several types of DSSCs. The cathodes made of graphite and platinum were supposed to be highly efficient because of their excellent electrical conductivity. However, the results in this study show that DSSCs using Ag-doped TiO_2/PVA nanofibers have the highest efficiency although the cathode was made of graphene oxide (GO) as the only semiconductor. It means that the Ag dopant and the electrospinning process fabricating nanofibers have positive effects on the efficiency of DSSCs. Hence, this is considered a successful application for this research.

CONCLUSION

In this study, Ag-doped TiO_2 NPs were successfully synthesized by the sol-gel method. Electrospun Ag-doped TiO_2/PVA nanofibers were prepared and applied as working electrodes of DSSCs. The Ag-doped TiO_2/PVA nanofibers were successfully prepared by an electrospinning method. The characteristics of the nanofibers were also analyzed. For DSSCs applications, when the Ag-doped TiO_2 content nanofibers increased from 60 to 100 mg/mL, the power conversion efficiency increased from 0.07 to 0.6%. Thus, the Ag-doped TiO_2/PVA nanofibers would inspire new developments in the design of highly efficient heterojunction structures in DSSCs and hybrid solar cell applications.

Acknowledgments

This work was funded by the Vietnam Ministry of Education and Training, under grant number B2021-TCT-05.

Received : Jun. 3, 2022 ; Accepted : Sep. 26, 2022

REFERENCES

[1] Takeshita T., Effect of the TiO_2 Surface Modification with 3-glycidyloxypropyltrimethoxysilane on the Aggregation of Cresyl Violet: Application to a Dye-Sensitized Solar Cell, *Mater. Chem. Phys.*, **286**: 126196 (2022).

[2] Conradie J., Polypyridyl Copper Complexes as Dye Sensitizer and Redox Mediator for Dye-Sensitized Solar Cells, *Electrochem. Commun.*, **134**: 107182 (2022).

[3] Van-Pham D.-T., Vien V.P., Nguyen T.Q.H., Nguyen H.N., Duong T.T.N., Ta N.D., Ngo T.N.M., Tran T.B.Q., Doan V.H.T., Fabrication of Electrospun $BaTiO_3$/chitosan/PVA Nanofibers and Application for Dye-Sensitized Solar Cells, *IOP Conf. Ser.: Earth Environ. Sci.*, **947 (1)**: 012017 (2021).

[4] Mahmood A., Khan S.U.-D., Rana U.A., Theoretical Designing of Novel Heterocyclic Azo Dyes for Dye Sensitized Solar Cells, *J. Comput. Electron.*, **13(4)**: 1033-41 (2014).

[5] Mahmood A., HussainTahir M., Irfan A., Khalid B., Al-Sehemi A.G., Computational Designing of

Triphenylamine Dyes with Broad and Red-Shifted Absorption Spectra for Dye-Sensitized Solar Cells

[6] Mahmood A., Recent Research Progress on Quasi-Solid-State Electrolytes for Dye-Sensitized Solar Cells, *J. Energy Chem.*, **24(6)**: 686-92 (2015).

[7] Mejica G.F.C., Unpaprom Y., Balakrishnan D., Dussadee N., Buochareon S., Ramaraj R., Anthocyanin Pigment-Based Dye-Sensitized Solar Cells with Improved pH-Dependent Photovoltaic Properties, *Sustain. Energy Technol. Assess.*, **51**: 101971 (2022).

[8] Shahzad N., Lutfullah, Perveen T., Pugliese D., Haq S., Fatima N., Salman S.M., Tagliaferro A., Shahzad M.I., Counter electrode Materials Based on Carbon Nanotubes for Dye-Sensitized Solar Cells, *Renew. Sust. Energ. Rev.*, **159**: 112196 (2022).

[9] Kabir F., Manir S., Bhuiyan M.M.H., Aftab S., Ghanbari H., Hasani A., Fawzy M., De Silva G.L.T., Mohammadzadeh M.R., Ahmadi R., Abnavi A., Askar A.M., Adachi M.M., Instability of Dye-Sensitized Solar Cells Using Natural Dyes And Approaches to Improving Stability – An Overview, *Sustain. Energy Technol. Assess.*, **52**: 102196 (2022).

[10] Kusumawati Y., Hutama A.S., Wellia D.V., Subagyo R., Natural resources for Dye-Sensitized Solar Cells, *Heliyon*, **7 (12)**: e08436 (2021).

[11] Aung S.H., Hao Y., Oo T. Z., Boschloo G., Kinetic Study of Carminic Acid and Santalin Natural Dyes in Dye-Sensitized Solar Cells, *J. Photochem. Photobiol. A: Chem.*, **325**: 1-8 (2016).

[12] Wang X., He G., Fong H., Zhu Z., Electron Transport and Recombination in Photoanode of Electrospun TiO_2 Nanotubes for Dye-Sensitized Solar Cells, *J. Phys. Chem. C*, **117(4)**: 1641-46 (2013).

[13] Zou X., Silva R., Huang X., Al-Sharab J.F., Asefa T., A Self-Cleaning Porous TiO_2–Ag Core–Shell Nanocomposite Material for Surface-Enhanced Raman Scattering, *Chem. Commun.*, **49 (4)**: 382-84 (2013).

[14] Wu W.-Y., Hsu C.-F., Wu M.-J., Chen C.-N., Huang J.-J., Ag–TiO_2 Composite Photoelectrode for Dye-Sensitized Solar Cell, *Appl. Phys. A*, **123(5)**: 357 (2017).

[15] Solaiyammal T., Muniyappan S., Keerthana B.G.T., Nemala S.S., Bhargava P., Murugakoothan P., Green Synthesis of Ag and the Effect of Ag on the Eficiency of TiO_2 Based Dye Sensitized Solar Cell, Using Multi-Thiophene Rings in π-Spacer, *Bull. Korean Chem. Soc.*, **36(11)**: 2615-20 (2015).
J. Mater. Sci. - Mater. Electron., **28 (20)**: 15423-34 (2017).

[16] Rho W.-Y., Kim H.-S., Chung W.-J., Suh J.S., Jun B.-H., Hahn Y.-B., Enhancement of power Conversion Efficiency with TiO_2 Nanoparticles/Nanotubes-Silver Nanoparticles Composites in Dye-Sensitized Solar Cells, *Appl. Surf. Sci.*, **429**: 23-28 (2018).

[17] Xu J., Wang G., Fan J., Liu B., Cao S., Yu J., g-C_3N_4 Modified TiO_2 Nanosheets with Enhanced Photoelectric Conversion Efficiency in Dye-Sensitized Solar Cells, *J. Power Sources*, **274**: 77-84 (2015).

[18] Ammar A.M., Mohamed H.S.H., Yousef M.M.K., Abdel-Hafez G.M., Hassanien A.S., Khalil A.S.G., Dye-Sensitized Solar Cells (DSSCs) Based on Extracted Natural Dyes, *J. Nanomater.*, **2019**: 1867271 (2019).

[19] Van-Pham D.-T., Phan T.Y.N., Tran V.B.L., Nguyen C.-N., Le M.N., Tran T.B.Q., Le T.C.T., Ngo T.N.M., Doan V.H.T., Electrospun Fe-doped TiO_2/chitosan/PVA Nanofibers: Preparation and Study on Photocatalytic and Adsorption Properties, *Mater. Lett.*, **326**: 132930 (2022).

[20] Andoshe D.M., Choi S., Shim Y.-S., Lee S.H., Kim Y., Moon C.W., Lee S.Y., Kim T., Park H.K., Lee M.G., A Wafer-Scale Antireflective Protection Layer of Solution-Processed TiO_2 Nanorods for High Performance Silicon-Based Water Splitting Photocathodes, *J. Mater. Chem. A*, **4 (24)**: 9477-85 (2016).

[21] Li S., Du P., Yang X., Yao L., Cao K., Enhanced Photocatalytic and Photoelectrochemical Activity via Sensitization and Doping Of Novel TiO_2 Nanowire/Nanoleaf Arrays: Dual Synergistic Effects between TiO_2–N and CdS–Mn, *RSC Adv.*, **6 (17)**: 13670-79 (2016).

[22] Zheng L., Yu X., Long M., Li Q., Humic Acid-Mediated Visible-Light Degradation of Phenol on Phosphate-Modified and Nafion-Modified TiO_2 Surfaces, *Chinese J. Catal.*, **38 (12)**: 2076-84 (2017).

[23] Wen J., Li X., Liu W., Fang Y., Xie J., Xu Y., Photocatalysis Fundamentals and Surface Modification of TiO_2 Nanomaterials, *Chinese J. Catal.*, **36 (12)**: 2049-70 (2015).

[24] Lim S.P., Lim Y.S., Pandikumar A., Lim H.N., Ng Y.H., Ramaraj R., Bien D.C.S., Abou-Zied O.K., Huang N.M.,

Gold–silver@ TiO_2 Nanocomposite-Modified Plasmonic Photoanodes for Higher Efficiency Dye-

[25] Gupta A.K., Srivastava P., Bahadur L., Improved Performance of Ag-Doped TiO_2 Synthesized by Modified Sol–Gel Method as Photoanode of Dye-Sensitized Solar Cell, *Appl. Phys. A*, **122(8)**: 1-13 (2016).

[26] Akhavan O., Lasting Antibacterial Activities of Ag–TiO_2/Ag/a-TiO_2 Nanocomposite Thin Film Photocatalysts Under Solar Light Irradiation, *J. Colloid Interface Sci.*, **336 (1)**: 117-24 (2009).

[27] Pakdel E., Daoud W.A., Sun L., Wang X., Reprint of: Photostability of Wool Fabrics Coated with Pure and Modified TiO_2 Colloids, *J. Colloid Interface Sci.*, **447**: 191-201 (2015).

[28] Saud P.S., Pant B., Twari A.P., Ghouri Z.K., Park M., Kim H.-Y., Effective Photocatalytic Efficacy of Hydrothermally Synthesized Silver Phosphate Decorated Titanium Dioxide Nanocomposite Fibers, *J. Colloid Interface Sci.*, **465**: 225-32 (2016).

[29] Wu L., Yu Y., Song L., Zhi J., M/TiO_2 (M= Au, Ag) Transparent Aqueous Sols and its Application on Polymeric Surface Antibacterial Post-Treatment, *J. Colloid Interface Sci.*, **446**: 213-17 (2015).

[30] Ren H.-T., Yang Q., Fabrication of Ag_2O/TiO_2 with Enhanced Photocatalytic Performances for Dye Pollutants Degradation by a pH-Induced Method, *Appl. Surf. Sci.*, **396**: 530-38 (2017).

[31] Yang Y., Ma Z., Xu L., Wang H., Fu N., Preparation of Reduced Graphene Oxide/Meso-TiO_2/AuNPs Ternary Composites and their Visible-Light-Induced Photocatalytic Degradation N of Methylene Blue, *Appl. Surf. Sci.*, **369**: 576-83 (2016).

[32] Sampaio D., Babu R.S., Costa H., De Barros A., Investigation of Nanostructured TiO_2 Thin Film Coatings for DSSCs Application Using Natural Dye Extracted from Jabuticaba Fruit as Photosensitizers, *Ionics*, **25 (6)**: 2893-902 (2019).

[33] Mozaffari S.A., Saeidi M., Rahmanian R., Photoelectric Characterization of Fabricated Dye-Sensitized Solar Cell Using Dye Extracted from Red Siahkooti Fruit as Natural Sensitizer, *Spectrochim. Acta, Pt. A: Mol. Biomol. Spectrosc.*, **142**: 226-31 (2015).

[34] Maurya I.C., Srivastava P., Bahadur L., Dye-Sensitized Solar Cell Using Extract from Petals of Sensitized Solar Cells, *Phys. Chem. Chem. Phys.*, **19(2)**: 1395-407 (2017).
Male Flowers Luffa Cylindrica L. as a Natural Sensitizer, *Opt. Mater.*, **52**: 150-56 (2016).

[35] Nguyen M.T., Vo Q.T., Ngo V.T., Vo Q M., Effect of Foaming Conditions on Foam Properties and Drying Behavior of Powder from Magenta (Peristropheroxburghiana) Leaves Extracts, *Horticulturae*, **8 (6)**: 546 (2022).

[36] Sujiono E.H., Zabrian D., Dahlan M., Amin B., Agus J., Graphene Oxide Based Coconut Shell Waste: Synthesis by Modified Hummers Method and Characterization, *Heliyon*, **6(8)**: e04568 (2020).

[37] He J., Du Y.-e., Bai Y., An J., Cai X., Chen Y., Wang P., Yang X., Feng Q., Facile Formation of Anatase/Rutile TiO_2 Nanocomposites with Enhanced Photocatalytic Activity, *Molecules*, **24(16)**: 2996 (2019).

[38] Soler-Illia G.d.A., Louis A., Sanchez C., Synthesis and Characterization of Mesostructured Titania-Based Materials Through Evaporation-Induced Self-Assembly, *Chem. Mater.*, **14 (2)**: 750-59 (2002).

[39] Yu J.C., Zhang L., Zheng Z., Zhao J., Synthesis and Characterization of Phosphated Mesoporous Titanium Dioxide with High Photocatalytic Activity, *Chem. Mater.*, **15 (11)**: 2280-86 (2003).

[40] Rao T.N., Babji P., Ahmad N., Khan R.A., Hassan I., Shahzad S.A., Husain F.M., Green Synthesis and Structural Classification of Acacia Nilotica Mediated-Silver Doped Titanium Oxide (Ag/TiO_2) Spherical Nanoparticles: Assessment of its Antimicrobial and Anticancer Activity, *Saudi J. Biol. Sci.*, **26 (7)**: 1385-91 (2019).

[41] Dhafina W.A., Salleh H., Daud M.Z., Ghazali M.S.M., Low Cost Dye-Sensitized Solar Cells Based on Zinc Oxide and Natural Anthocyanin Dye From Ardisia Elliptica Fruits, *Optik*, **172**: 28-34 (2018).

[42] Lin S.-J., Lee K.-C., Wu J.-L., Wu J.-Y., Plasmon-Enhanced Photocurrent in Dye-Sensitized Solar Cells, *Sol. Energy.*, **86 (9)**: 2600-05 (2012).

[43] Zhang X., Thavasi V., Mhaisalkar S., Ramakrishna S., Novel Hollow Mesoporous 1D TiO_2 Nanofibers as Photovoltaic and Photocatalytic Materials, *Nanoscale*, **4 (5)**: 1707-16 (2012).

[44] Swarnkar A., Sahare S., Chander N., Gangwar R.K., Bhoraskar S., Bhave T.M., Nanocrystalline Titanium Dioxide Sensitised with Natural Dyes for Eco-Friendly Solar Cell Application, *J. Exp. Nanosci.*, **10 (13)**: 1001-11 (2015).

[45] Chang H., Lo Y.-J., Pomegranate Leaves and Mulberry Fruit as Natural Sensitizers for Dye-Sensitized Solar Cells, *Sol. Energy.*, **84 (10)**: 1833-37 (2010).